Research article

Fenghao Sun, Hui Li*, Shanshan Song, Fei Chen, Jiawei Wang, Qiwen Qu, Chenxu Lu, Hongcheng Ni, Botao Wu, Hongxing Xu and Jian Wu*

Single-shot imaging of surface molecular ionization in nanosystems

https://doi.org/10.1515/nanoph-2021-0172
Received April 17, 2021; accepted June 29, 2021;
published online July 12, 2021

Abstract: Using single-shot velocity map imaging technique, explosion imaging of different ion species ejected from 50 nm SiO_2 nanoparticles are obtained excitedly by strong near-infrared and ultraviolet femtosecond laser fields. Characteristic momentum distributions showing forward emission of the ions at low excitation intensities and shock wave behaviors at high intensities are observed. When the excitation intensity is close to the dissociative ionization threshold of the surface molecules, the resulting ion products can be used to image the instant near-field distributions. The underlying dynamics of shock formation are simulated by using a Coulomb explosion model. Our results allow one to distinguish the ultrafast strong-field response of various molecular species in nanosystems and will open a new way for further exploration of the underlying dynamics of laser-and-nanoparticle interactions.

Keywords: nanoparticle; shock wave; strong-field ionization; surface molecules; velocity map imaging.

1 Introduction

Interactions between nanosystems and light fields play crucial roles in the development of laser machining [1–3], cancer treatment [4, 5], photocatalysis [6], etc. When excited with femtosecond laser fields, near field enhancement can be induced around the nanostructures that changes dramatically in femtosecond time scales. The induced near field initiate the ionization processes, while the produced nanoplasma can in turn tailor the local field distributions. The spatiotemporally highly confined dynamics of the strong coupling between the ultrafast laser field and nanoplasmonic systems is of great complexity and has not yet been fully understood.

Advanced detection methods are required to explore such processes. Recently, aerosol nanoparticle sources in vacuum systems have been implemented to explore their interactions with femtosecond laser pulses [7–10]. The generated charged fragmentation can be detected by velocity map imaging (VMI) [7–10], time of flight (TOF) spectroscopy [11–13], and even reaction microscopy [14, 15]. Compared with optical spectroscopy where the nanostructures are suspended in solutions or on substrates, the use of a vacuum nanoparticle source can significantly avoid the influence from the environment. Moreover, the nanoparticle interacting with the femtosecond pulses are constantly refreshing when utilizing a free-flying source. Combined with the single-shot detection method, the averaging effect in the measurement can be prevented. Even so, limited information can be extracted from the commonly used photoelectron imaging technique due to the fact that the final distribution of the electrons can be affected by many aspects, e.g. elastic and inelastic scatterings [10, 16–18], charge interactions [19, 20]. Furthermore, it is hard to distinguish the electrons released from different species of the target. In contrast, by detection of a specific ion species one can learn more details of the interactions. For instance, the reaction nanoscope shows impressive potential for exploring nanoparticle dynamics, by performing coincidence measurements on the ions generated from nanoparticles [14].

On the other hand, although the sample is very well processed, there are usually some residue molecules attached to the nanomaterial surfaces. The influence of these "surface" molecules is ignored in most cases. However, they can play crucial roles in the interactions between

***Corresponding authors: Hui Li**, State Key Laboratory of Precision Spectroscopy, East China Normal University, Shanghai 200241, China, E-mail: hli@lps.ecnu.edu.cn; and **Jian Wu**, State Key Laboratory of Precision Spectroscopy, East China Normal University, Shanghai 200241, China; Collaborative Innovation Center of Extreme Optics, Shanxi University, Taiyuan, Shanxi 030006, China; and CAS Center for Excellence in Ultra-intense Laser Science, Shanghai 201800, China, E-mail: hli@lps.ecnu.edu.cn (H. Li), jwu@phy.ecnu.edu.cn (J. Wu). https://orcid.org/0000-0003-0927-8124 (H. Li)
Fenghao Sun, Shanshan Song, Fei Chen, Jiawei Wang, Qiwen Qu, Chenxu Lu, Hongcheng Ni, Botao Wu and Hongxing Xu, State Key Laboratory of Precision Spectroscopy, East China Normal University, Shanghai 200241, China. https://orcid.org/0000-0003-0210-5204 (F. Sun). https://orcid.org/0000-0003-4924-0921 (H. Ni)

nanostructures and strong laser fields. It was recently demonstrated that the proton emission from the surface of 300 nm SiO_2 nanoparticle dimers produce distinct momentum features which can be used to make identification between single nanoparticle and clusters as long as the propagation effects are not significant in single particles [15]. Moreover, the influence of surface molecules should be handled carefully when studying the processes excited by strong laser fields. In many cases, the surface molecules can interact with the strongest part of the enhanced near field. It is of great probability that the molecules attached to the nanosurfaces are firstly ionized and can impact significantly on the succeeding interactions between the incident light and nanosystems. In this work, we focus on small silica nanoparticles (with diameters of around 50 nm) wrapped by water and silanol molecules. Femtosecond pulses at central wavelengths of 800 and 400 nm are used to excite the free-flying nanoparticles in the vacuum chamber. The momentum distributions of the resulting ions from both the surface molecules and the nanoparticles are detected in a single-shot VMI apparatus, which are individually gated according to their distinguished arriving time at the detector. In addition to previous works [8, 14], we found that the ion products from the surface molecules can be used to study both the instantaneous near-field distributions and the shock wave processes.

2 Methods

The measurement was performed in an ultrahigh vacuum chamber of VMI apparatus [21] where a nanoparticle source was implemented [22]. As schematically illustrated in Figure 1(A), the femtosecond laser pulses from a Ti:sapphire amplification system (35 fs @ 800 nm, 1 kHz) were focused on the free-flying aerosol of 50 nm silica nanoparticles by a focusing lens (f = 500 mm). Femtosecond pulses at the central wavelength of 400 nm obtained from frequency doubling of the incident 800 nm pulses in a piece of Beta-Barium Borate crystal were also used to illuminate the nanoparticles. The generated ions in the interactions of femtosecond laser pulses with the nanoparticle systems were guided toward a microchannel plate (MCP)/phosphor detector at the end of the spectrometer and the induced images were detected by a high-speed single-shot camera (Phantom V410). In this work, a fast high-voltage switch with a tunable time delay with respect to the laser pulse trigger was applied to the MCP thus different ion species generated in the nanosystem can be distinguished by their arriving times on the detector. The silica suspension was prepared by template method [23] to avoid the pollution from carbon fragments which usually exist in other organic preparation methods and the concentration was diluted to 0.02 g/L in water to avoid the formation of large clusters. The nanoparticles were aerosolized by the atomizer with Ar gas (1.5 bar). Although most of the water molecules could be removed when the nanoparticles going through a diffusion dryer (MD-700 Nafion™ Dryer; Perma Pure, LLC), there were still some water molecules attached to the nanospheres when they were injected into the interaction chamber by an aerodynamic lens system. Due to the fact that the spacing between individual nanoparticles was large, it is estimated that one nanoparticle can be illuminated for every 50 laser shots on average. The angle-resolved momentum distributions of the H^+ ions from ionization of the surface molecules as well as the Si^+ ions generated from the silica nanoparticles were explicitly measured in a single-shot manner. Each nanoparticle may experience a different laser intensity depending on where it was irradiated in the laser focus [9]. Thus the single-shot imaging technique was capable to reveal the underlying mechanism which was usually obscure in the integrating detection methods. The intensities of the linearly polarized laser fields in the reaction region were estimated by examining the momentum shifts of the above-threshold ionization photoelectrons from strong-field ionization of Xe along the laser polarization direction [24, 25]. Atomic units (a.u.) were used throughout this paper unless otherwise indicated.

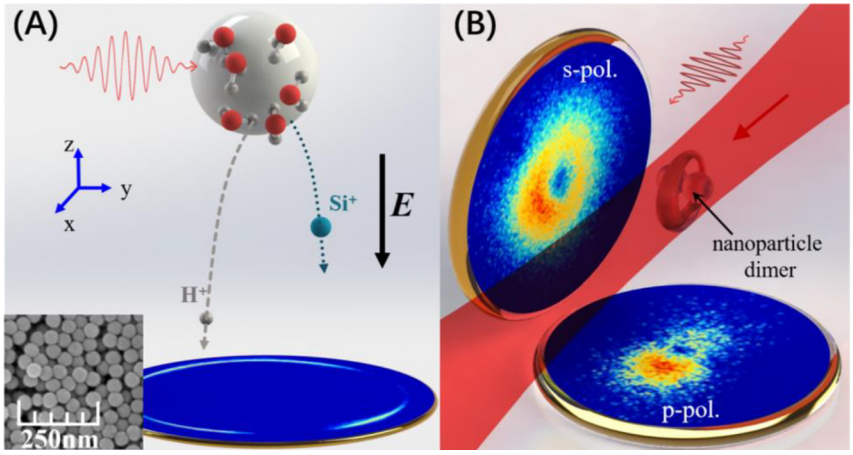

Figure 1: (A) Schematic drawing of the experimental apparatus. The black arrow indicates the static electric field in the velocity map imaging (VMI) spectrometer, and the blue arrows show the coordination of the experiment. The inserted image on the lower-left corner is the scanning tunneling electron microscopy (SEM) image of the 50 nm SiO_2 nanoparticles. (B) Schematic illustration of the momentum distributions of the protons ejected from the surface molecules under low-intensity excitation projected onto two orthogonal planes. The nanoparticle dimer is oriented along the laser polarization direction.

3 Results and discussions

3.1 Forward focusing of photoions from nanoparticle dimers

TOF measurements showed dominating H^+ and Si^+ ion products in the ion emissions, where the H^+ ions can be generated from the surface molecules (contains water and to some extent silanols) while the Si^+ ions are from the ionization of SiO_2 nanoparticles. Single-shot momentum distributions were obtained explicitly for both the H^+ and Si^+ ion emission under low excitation intensities at both 800 and 400 nm, where forward focusing was recognized (as shown in Figures 1B and 2). Numerous studies have indicated that near-field enhancement can play a key role when nanoparticles are exposed to laser fields at comparable intensities [10, 11, 15, 17, 26, 27]. Based on Mie theory [28], the characteristic response of a nanoparticle in a laser field is highly related to the size parameter, i.e. $\rho = \pi d/\lambda$, where d is the diameter of the nanoparticle and λ is the excitation wavelength. A forward focusing can be expected for the single-particle excitation when the size parameter is approaching or larger than unity, which is not the case in our experiment. Sample characterization using scanning tunneling electron microscopy indicated an averaging size of around 50 nm with a size deviation of about 5% (shown in the inserted image in Figure 1A). The individual silica nanosphere used in this work did not exhibit apparent propagation effects when interacts with femtosecond pulses at 800 and 400 nm [10]. Recent work reported that a clear asymmetric momentum distribution can be found in the proton emission in the propagation direction for nanoparticle clusters [15]. This could be a general case since there is a probability that clusters can be transmitted to the interaction regions through the aerosol source and aerodynamic lens. Actually, the aerodynamic lens in our setup is designed with optimized transition probability for particles with a diameter of around 100 nm. This size coincided with the dimension of the dimer system consisting of two 50 nm silica nanospheres. Therefore we think that the transmission rate for the dimer in the present work is considerable, while the rate for larger clusters drops quickly. We examined the situation in our case by the Finite-Difference Time-Domain (FDTD) simulations, and the results in Figure 3 showed that the enhanced near field excited by linearly polarized 800 and 400 nm fs pulses at low excitation intensities exhibiting an asymmetric distribution along the laser propagation for oriented nanoparticle dimers. As shown in Figure 3 (and schematically illustrated in Figure 1B), when the two nanospheres are oriented parallel to the laser polarization in a linearly polarized optical field, the maximum near-field strength represents a donut-shaped distribution around the contacting area of the nanospheres in a dimer system. A magnitude of 0.5% (or 5%) enhancement of the optical field can be revealed in the forward direction of the laser propagation with respect to the backward direction in the asymmetry plot for 800 nm (or 400 nm) (as shown in Figures 3B and D). Here, the asymmetry parameter was calculated by subtracting the field strength in the backward direction from that in the forward direction and dividing by their summation. The FDTD calculations also showed that only those dimer systems oriented parallel to the light polarization direction or exhibiting small deviations from the above orientation condition could address the observed asymmetric distributions along the light propagation direction. A maximum enhancement factor of about two could be obtained between the nanospheres in a dimer system (as shown in Figures 3A and C) where the effective electric field strength acting on the surface molecules can be close to their dissociative ionization thresholds. In this case, a tiny intensity difference can cause an amplified asymmetry in the ion emissions along the light propagation direction [29]. The observed H^+ ion emissions for both the *p*- and *s*-polarizations and at two excitation wavelengths (shown in Figures 2A–D) conformed to the hypothesis of reaction from dimer systems. In the low-intensity regime, the dissociative ionization of the surface molecules was dominated by the instantaneous near field enhancement thus the resulting momentum distributions of proton inherit the characteristics from the near fields. The momentum distributions for the Si^+ ion emission at 800 and 400 nm excitations showed a forward focusing effect at the intensity of 30 TW/cm^2, which were shown in Figures 2E and F. The threshold excitation intensity for one to observe a considerable Si^+ ion signal was higher than that required for the H^+ ions. Despite the deviation from the dissociative ionization potentials for different molecules, the surface molecules sitting outside the nanospheres experience the most enhanced near field, while the atoms and molecules inside the nanosystem are excited by a weaker local field. As can be seen in Figures 3A and C, the fields inside the nanoparticle drop below unity quickly leaving a large gradient near the surface. In addition, two hollow cores were observed close to the zero momentum in the Si^+ ion emission (e.g. the image shown in Figure 2E). One possible explanation could be that the Coulomb repulsion from the ionization-produced spatially

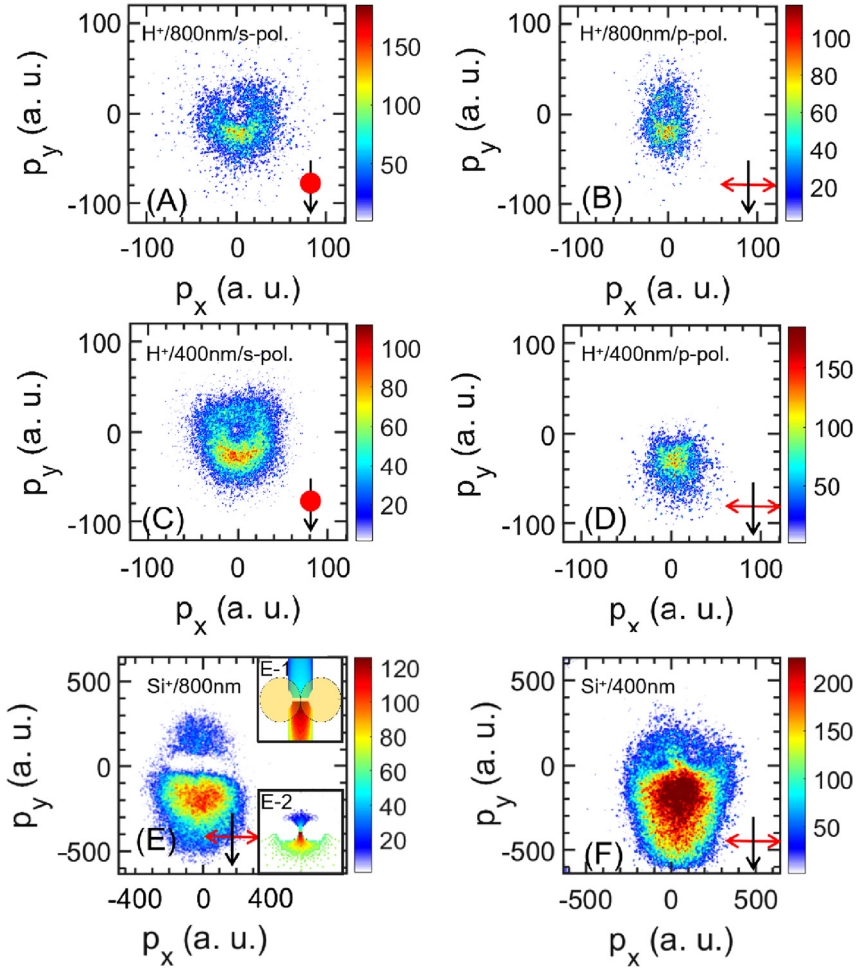

Figure 2: The single-shot momentum distributions for the ions ejected from the nanoparticle systems at the low intensities. The color scale represents the intensity profile obtained on the CMOS detector. (A–D) The momentum distribution for the H^+ ions at excitation intensity of 17 TW/cm^2. As indicated in the figures, the pulses are *s*- or *p*-polarized, at 800 or 400 nm. The black and red arrows indicate the laser propagation and polarization directions, respectively. The red dots in (A, C) represent the laser polarization perpendicular to the *xy* plane (E, F) The momentum distribution for the Si^+ ions excited by *p*-polarized femtosecond laser pulses at 30 TW/cm^2 at 800 nm and at 400 nm, respectively. The inserted figures on the upper and lower right corner in (E) are the initial charge distribution in the *xy* plane and the corresponding calculated momentum distributions.

separated nanoplasmas caused such distinct nonzero hollow-core momentum distributions. When the femtosecond pulses illuminated the nanoparticle dimer and caused sufficient dissociative ionization, the generated charges from one nanoparticle on the one side felt the Coulomb repulsion from the ionized nanoparticle on the other side. As a result of this, the generated ions could be exerted with an outward force, therefore, exhibiting the "hollow-core structure" with nonzero momentum. To make this clear the process was simulated based on a simple classical model involving ionization and charge dynamics. In the simulation, the initial distribution of the charged particles was estimated according to the near field profile. In the low-intensity regime studied here, the ion yields generated in the two-dimensional (2D) plane at $z = 0$ nm accounted for a major part of the final three-dimensional (3D) momentum distributions. Based on this, the simulation was carried out in 2D for simplicity. The maximum charge density was set to be close to the connection point of the two nanospheres in the dimer. As is shown in the inserted figure in Figure 2(E-1), the initial charge density follows a quadratic decrease along the *x*-axis and an exponential decrease along the *y*-axis. Some of the initial ion trajectories start inside the silica nanoparticles from a depth of about 10 nm. To reach a better agreement between the simulation and the observed data, two effective positive charges (representing the ionization created nanoplasmas which were left behind the outgoing ions) were placed at two effective positions on the *x*-axis which were to some extent shifted to the origin from the center of the nanoparticle. The exact effective positions were mainly determined by the degree of ionization of the dimer system. The following dynamics of the Si^+ ions were calculated using Newtonian equations of motion by considering the Coulomb interactions. The calculated momentum distribution of Si^+ ions showed a clear "hollow-core" structure (see the inserted figure in Figure 2(E-2)). Such structure observed under this laser intensity level is mainly caused by the Coulomb repulsion of the ionization-created nanoplasmas separated in space.

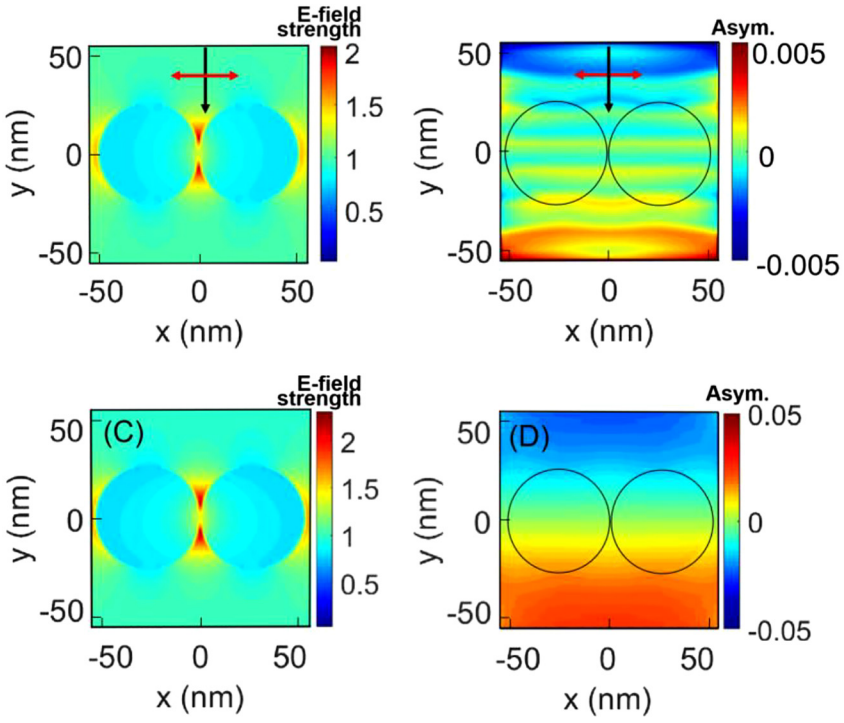

Figure 3: Finite Difference Time Domain (FDTD) calculations (using Lumerical) of the induced near fields of silica nanoparticle systems.
(A) The distribution of the maximum near field strength around a nanoparticle dimer consisting of two 50 nm SiO_2 nanoparticles, excited by femtosecond laser pulses at 800 nm. The color scale represents the enhancement factor of the field amplitude. The black and red arrows indicate the laser propagation and polarization directions, respectively. (B) The calculated asymmetry of the field strength from (A) along the laser propagation direction for a dimer system. The black circles indicate the dimer. (C) and (D) are similar to those of (A) and (B) but for the excitation at 400 nm.

In our experiment, single-shot images with similar distributions occupied over 80% of the valid images. Such orientation-dependent reactions in nanoparticle dimers dominated the interaction at low laser intensities. The influence from the background gases was also characterized and could be neglected. The laser intensities used here were too weak to cause any ionization of the background gases without the near field enhancement effect. From the above, we can see that in the case of low-intensity excitation, the enhanced near field of an individual small silica nanoparticle (with $\rho << 1$) is not sufficient to cause considerable ionization event. The observed ion signals are dominated by the emission from nanoparticle dimers by comparing the ion momentum distributions with the calculated near-field profiles. As a matter of fact, no matter how carefully the sample is prepared, there will always be some polymers being transmitted to the interaction region [16]. Since the molecules adhering to the nanoparticle surface first experience the most enhanced near field, the dissociative ionization products of the surface molecules can potentially image the instant near field distributions at low laser intensities.

3.2 Shock waves in the H^+ and Si^+ ion emissions

When silica nanospheres interact with femtosecond pulses at intensities beyond the dielectric breakdown, a highly nonlinear response will take place followed by complex coupling dynamics. The nonlinear response at high intensity is tightly connected with plasma formation [30], ultrafast metallization [31, 32], generation of high energy electrons [13], and multiply charged ions [33, 34]. In this work, the formation of shock waves were distinguished in the SiO_2 nanospheres irradiated by intense femtosecond laser pulses at 800 and 400 nm. The momentum distributions of either the H^+ ions (ionized from the surface molecules) or the Si^+ ions (generated from ionization of silica nanospheres) were explicitly mapped utilizing a single-shot momentum imaging technique. As can be seen in Figures 4A–C, distinct momentum distributions with a sharp ridge were observed in addition to a broad distribution for all the emission directions, representing a shock-wave feature in both the H^+ and Si^+ ion emissions [8]. Particularly, the shock formation from surface molecules in individual nanoplasma manifested as a radial momentum distribution that can be fitted by two Gaussian functions, of which the broader Gaussian profile was from typical nanoplasma expansion while the narrower one represented the shock wave (as shown in Figures 4E and F). From the Gaussian fits, we could see that the sharp ring showing in Figure 4A has a width of about 2.9 a.u. at the central momentum of about 90 a.u., with a momentum spreading of less than 5%. The data shown in Figure 4 were all obtained at the intensity of 100 TW/cm^2. As a matter of fact, clear shock wave formation was observed in the H^+

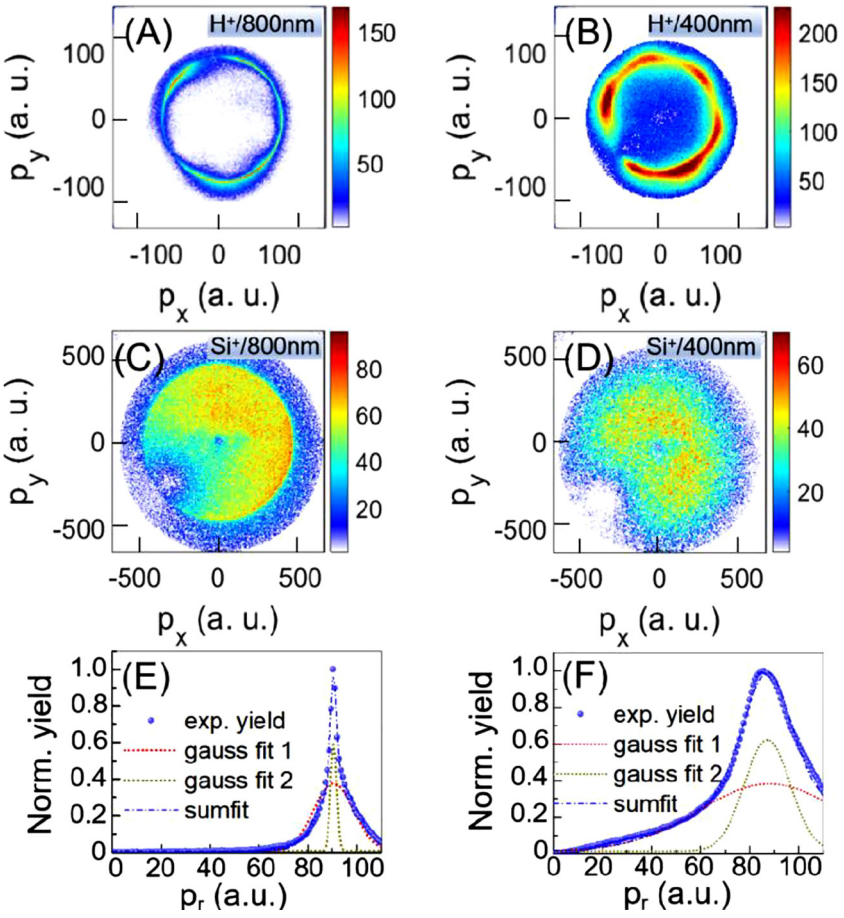

Figure 4: (A) The momentum distribution of the H^+ ion emission from the nanoparticle system irradiated at the excitation intensity of 100 TW/cm^2 at 800 nm. The black and red arrows indicate the laser propagation and polarization directions, respectively. (B) Similar to (A) but for the excitation at 400 nm. (C) and (D) are similar to those of (A) and (B) but are obtained for the Si^+ ions. (E) and (F) are the radial momentum distributions of the H^+ ions (shown in A and B) fitted by two Gaussian functions. The blue scattered bullets show the experimental yield. The blue dash-dot curve represents the 2-Gaussian fitting result. The red and dark yellow dashed curves are the separated Gaussian fitting results, representing the plasma expansion and the shock wave, respectively.

momentum distributions at excitation intensity of 50 TW/cm^2 at 800 nm (data not shown here), exhibiting a similar angular distribution compared to Figure 4A, but with a smaller central momentum at around 66 a.u. It needs to be noted that the H^+ momentum distribution shown here was only a thin slice of the 3D momentum distribution since a short time window was applied on the detector. We also observed shock formation in the Si^+ ion emission at 100 TW/cm^2 (Figure 4C), where the sharp ridge formed at a large momentum of about 470 a.u. We offer a possible explanation regarding the broad momentum distribution extending from about 0 toward ca. 500 a.u. as follows: when the highly nonlinear response in the nanosystem is so strong that it becomes sufficient for the ionization to take place in the bulk, the Si^+ ions will be emitted from different depths in the nanoparticles and a wide range of momentum distribution can be formed. Early work has also shown that by using an additional excitation beam prior to the pump pulse, and by properly controlling the time delay between the two pulses, the density profile of the nanoplasma can be optimized for the formation of shocks [8]. In this work, a single beam was used to ignite individual SiO_2 nanoplasmas and the shock behaviors could be obtained in the momentum distributions in a couple of ion products at excitation wavelengths of both 800 and 400 nm. Nevertheless, the shock formed in H^+ ions at 400 nm excitation showed a broader momentum profile compared to that obtained at 800 nm, which can be seen in the Gaussian fitting results in Figure 4F. The shock wave exhibited a width of about 22 a.u., corresponding to a momentum spreading of about 25%. We did not find a shock signal in the Si^+ ion emission at 400 nm. The different responses at the two wavelengths can be attributed to the distinct absorption cross-sections of the SiO_2 nanoparticles at a specific wavelength which can change dramatically the following density dynamics [8]. Apparently, the shock formation in the case of 400 nm excitation was not optimized here, which can be potentially improved by double-pulse excitation.

Simulations based on the Coulomb explosion model [35] were carried out to explore the mechanism for shock formation in the strong field excitation of 50 nm SiO_2

nanoparticles. In our model, the initial nanoplasma was defined with a certain profile of charged particles. The initial density profile and the initial velocity distribution for the charged particles were written as

$$D(r_0) = (3/4\pi) * (R_0^3 N_\Sigma) \Big/ (r_0^3 + R_0^3)^2 \quad (1)$$

$$V_0(r_0) = k_1 * \exp(r_0/k_2) - k_1 \quad (2)$$

Here, $N_\Sigma = 4000$ was the total number of charged particles in the simulation, r_0 was the initial position for the charged particle, R_0 = 50 nm was the effective radius of the excited nanoparticle (please note here that the effective size of the excited nanoparticle is to some extent larger than the initial size of the nanoparticle. The variation of this parameter in a certain range (e.g. [40, 60]) will not affect the calculated results dramatically.), k_1, k_2 were two constant parameters that determined the decay rate of particle velocity from the outermost layer to the center of the nanoplasma. The initial nanoplasma was defined with a density profile which was decreased along the escaping direction [35] and the initial velocity distribution was given as a monotonically increasing function of radius. The maximum momentum of ions was set to be 120 a.u. in our simulation according to the measured H^+ data, and thus the two parameters k_1 and k_2 could be derived. The generated H^+ ions from surface ionization were evolved in a Coulomb field exerted by the charges generated in the silica nanoparticle. The classical trajectories of the ions thus can be obtained based on energy conservation. Figures 5A and B showed the momentum and ion density at different radius for three instances. The normalized ion yield as a function of momentum shown in Figure 5C indicated that a stable shock formation could be realized at around 70 ps after the excitation, the momentum of which agreed with the measured value. In our work, the images that we obtained on the detector were 2D projections of the final state momentum distributions of the flying ions, corresponding to the calculated stable state results. The 70 ps formation time in the plasma expansion was in the same order compared to the results reported in the previous work [8]. Theoretical simulations showed that the exceeding of the faster moving inner ions with respect to the slower preceding ones could generate a critical surface with high charge density, which eventually caused a leading shock wave.

Distinct angular distributions were identified in the H^+ emission for both the 800 nm and the 400 nm excitation at high laser intensity (as shown in Figures 4A, B, and 6). We

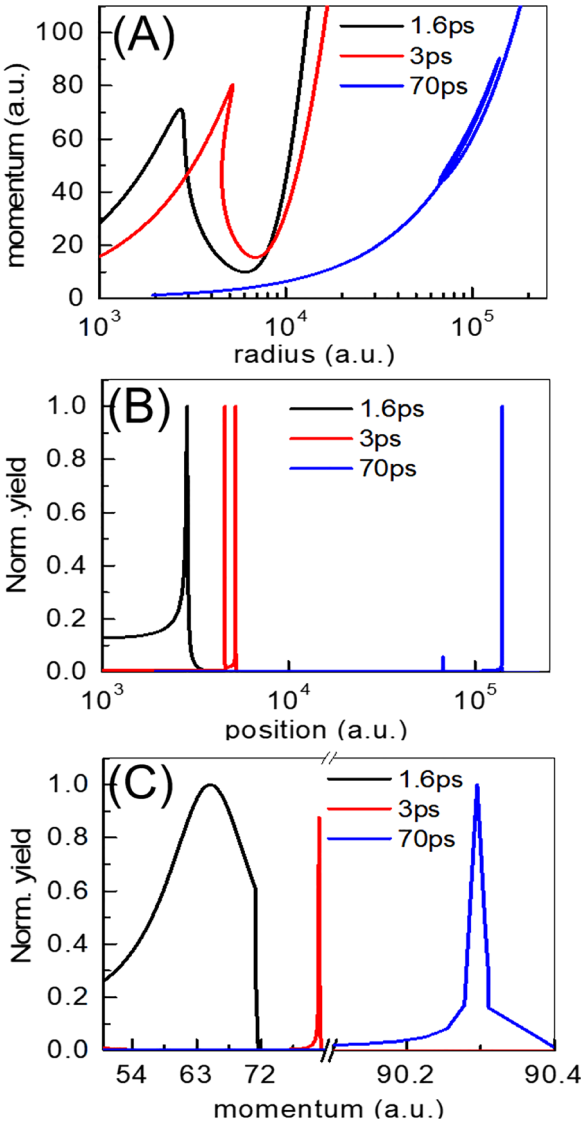

Figure 5: Calculated results at three distinct moments (1.6, 3, and 70 ps) showing the mechanism of the shock formation in the H^+ ion emission.
(A) The momentum of the flying ions at the different radius. Here the center of the nanosphere is defined as the origin of the *x*-axis. (B) The normalized ion yields as a function of radius. (C) The normalized ion yields as a function of momentum. A stable sharp peak is formed at a final momentum of around 90 a.u. at about 70 ps.

have made a statistical analysis of the angular distributions obtained at this intensity region for the two laser wavelengths. Theoretically, if the excitation laser intensity is the same, both the total ion yield Y_{total} and the momentum with the maximum counts P_m would be comparable. These two parameters (Y_{total} and P_m) derived from each single-shot image were sorted and the statistical

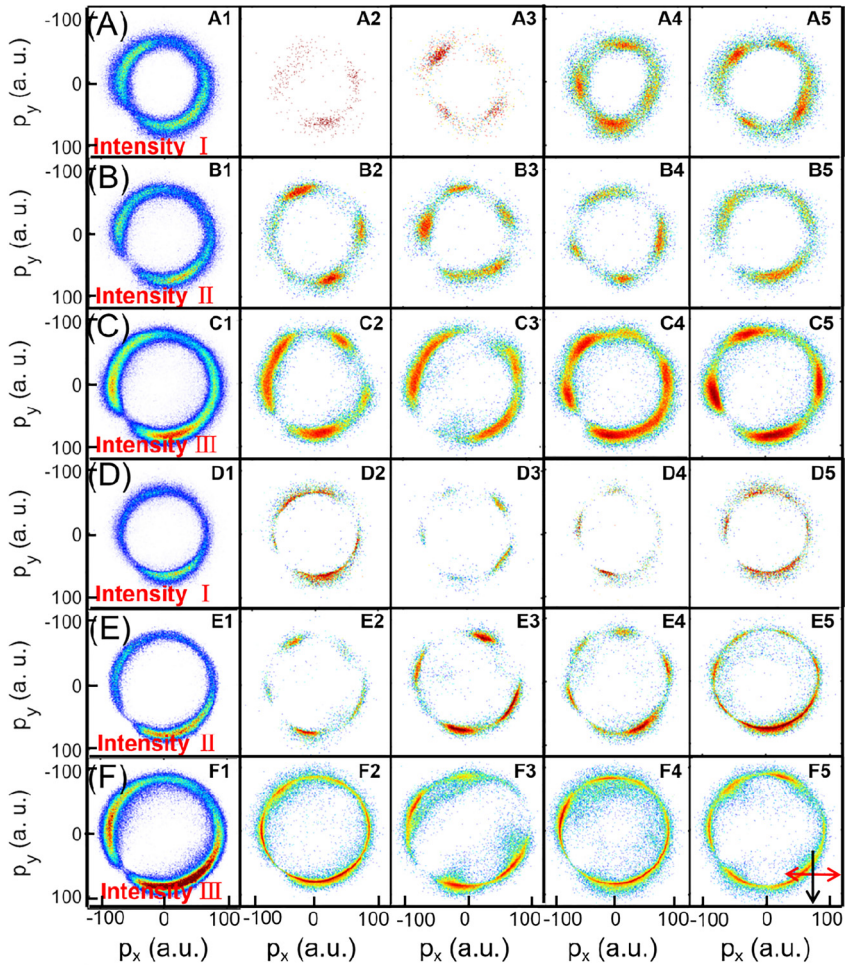

Figure 6: (A–C) show the integrated (the first column) and the single-shot (the 2nd to the 5th column) H^+ momentum distributions at three laser intensities at 400 nm. The three intensity regions correspond to the areas marked by I, II, and III in Figure 7(A). (D–F) Similar to (A–C) but obtained at 800 nm. The black and red arrows at the bottom right of the figure indicate the laser propagation and polarization directions, respectively.

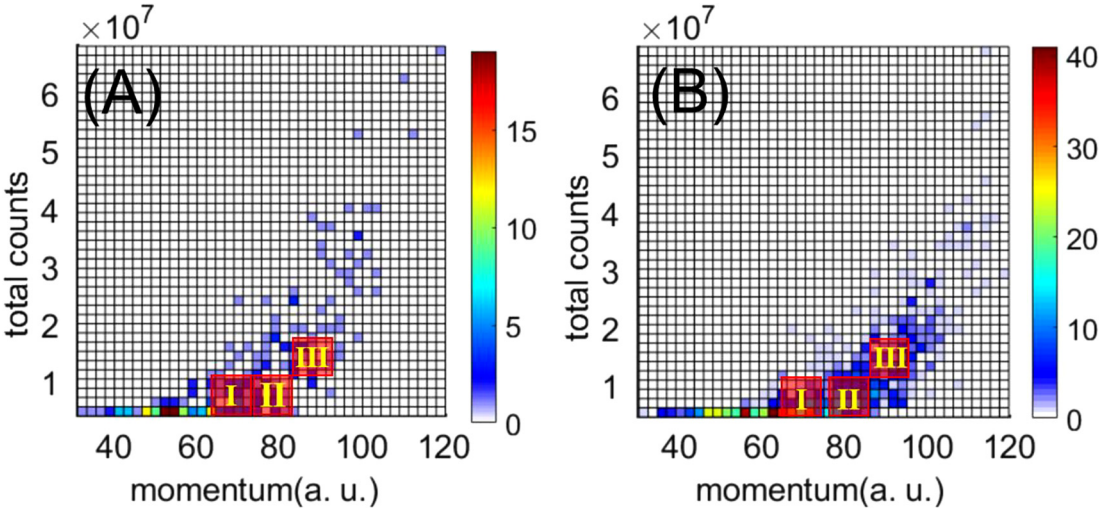

Figure 7: (A) and (B) are statistics of thousands of single-shot measurements sorted by the momentum of the maximum counts and the corresponding total counts of the image, at 400 and 800 nm, respectively. The color bar represents the number of images satisfying the related parameters. Three regions marked I, II, and III are selected corresponding to three distinct intensity conditions.

results were shown in Figure 7. For each statistics, three different regions, marked by I, II, and III were selected corresponding to data obtained at distinct laser intensities. The integrated angular distributions for each selected region can be seen in the first column in Figure 6. Despite the excitation wavelength, it was shown that the integrated angular distributions at different laser intensities exhibiting similar profiles, which could be mainly caused by the detection efficiency deviation of the detector when the ions hit at different positions. The different angular features obtained for each single-shot momentum distribution might be rooted from the diversity of individual nanoparticles [29].

4 Conclusions

Utilizing the single-shot VMI technique, the momentum distributions of different ion species generated from the surface molecules and from the SiO_2 nanoparticles were explicitly imaged by gating on their arriving times at the detector. Different reaction mechanisms were extracted when the 50 nm nanoparticles interacting with femtosecond laser fields at different intensities and wavelengths. At low driven intensities, where a single nanoparticle could not generate considerate ionization events, the observed ion signals were dominated by reactions in oriented nanoparticle dimers close to the molecular dissociative ionization thresholds. A forward focusing effect could be observed in the ion momentum maps which was determined by the induced near field distribution. At relatively high laser intensities where the nanoparticles were highly ionized to produce nanoplasma, the ionization fragments from the surface molecules showed a distinct momentum profile representing the shock wave formations. The underlying mechanism of which was revealed by comparing to the simulations based on the Coulomb explosion model. This work paves the way for further exploration of the underlying dynamics of interactions between strong laser fields and nanosystems, by potentially implementing time-resolved investigations.

Acknowledgments: We thank Dr. Qingcao Liu for his assistance in setting up the nanoparticle source. We thank Prof. Vinod Kumarappan for sharing with us the hit-finding code in the early stage.

Author contributions: All the authors have accepted responsibility for the entire content of this submitted manuscript and approved submission.

Research funding: This work was supported by the National Key R&D Program of China (Grant No. 2018YFA0306303); the National Natural Science Fund (Grant Nos. 92050105, 11834004, 11621404, 11761141004, 11704124); the Project supported by the Shanghai Committee of Science and Technology, China (Grant Nos. 19ZR1473900, 19JC1412200); Shanghai Municipal Science and Technology Major Project.

Conflict of interest statement: The authors declare no conflicts of interest regarding this article.

References

[1] L. Englert, M. Wollenhaupt, L. Haag, C. Sarpe-Tudoran, B. Rethfeld, and T. Baumert, "Material processing of dielectrics with temporally asymmetric shaped femtosecond laser pulses on the nanometer scale," *Appl. Phys. A Mater. Sci. Process*, vol. 92, pp. 749–753, 2008.

[2] P. Balling and J. Schou, "Femtosecond-laser ablation dynamics of dielectrics, basics and applications for thin films," *Rep. Prog. Phys.*, vol. 76, p. 036502, 2013.

[3] K. M. Tanvir Ahmmed, C. Grambow, and A. M. Kietzig, "Fabrication of micro/nano structures on metals by femtosecond laser micromachining," *Micromachines*, vol. 5, no. 4, pp. 1219–1253, 2014.

[4] V. K. Pustovalov, A. S. Smetannikov, and V. P. Zharov, "Photothermal and accompanied phenomena of selective nanophotothermolysis with gold nanoparticles and laser pulses," *Laser Phys. Lett.*, vol. 5, pp. 775–792, 2008.

[5] R. Lachaine, E. Boulais, and M. Meunier, "From thermo- to plasma-mediated ultrafast laser-induced plasmonic nanobubbles," *ACS Photonics*, vol. 1, pp. 331–336, 2014.

[6] D. Beydoun, R. Amal, G. Low, and S. McEvoy, "Role of nanoparticles in photocatalysis," *J. Nanoparticle Res.*, vol. 1, pp. 439–458, 1999.

[7] K. R. Wilson, S. Zou, J. Shu, et al., "Size-dependent angular distributions of low-energy photoelectrons emitted from NaCl nanoparticles," *Nano Lett.*, vol. 7, pp. 2014–2019, 2007.

[8] D. D. Hickstein, F. Dollar, J. A. Gaffney, et al., "Observation and control of shock waves in individual nanoplasmas," *Phys. Rev. Lett.*, vol. 112, p. 115004, 2014.

[9] J. A. Powell, A. M. Summers, Q. Liu, et al., "Interplay of pulse duration peak intensity and particle size in laser-driven electron emission from silica nanospheres," *Opt. Express*, vol. 27, pp. 27124–27135, 2019.

[10] S. Zherebtsov, T. Fennel, J. Plenge, et al., "Controlled near-field enhanced electron acceleration from dielectric nanospheres with intense few-cycle laser fields," *Nat. Phys.*, vol. 7, p. 656, 2011.

[11] T. Fennel, K. H. Meiwes-Broer, J. Tiggesbäumker, et al., "Laser-driven nonlinear cluster dynamics," *Rev. Mod. Phys.*, vol. 82, p. 1793, 2010.

[12] J. Passig, R. Irsig, N. X. Truong, T. Fennel, J. Tiggesbäumker, and K. H. Meiwes-Broer, "Nanoplasmonic electron acceleration in silver clusters studied by angular-resolved electron spectroscopy," *New J. Phys.*, vol. 14, p. 085020, 2012.

[13] J. Passig, S. Zherebtsov, R. Irsig, et al., "Nanoplasmonic electron acceleration by attosecond-controlled forward rescattering in silver clusters," *Nat. Commun.*, vol. 8, p. 1181, 2017.

[14] P. Rupp, C. Burger, N. Kling, et al., "Few-cycle laser driven reaction nanoscopy on aerosolized silica nanoparticles," *Nat. Commun.*, vol. 10, p. 4655, 2019.

[15] P. Rosenberger, P. Rupp, R. Ali, et al., "Near-field induced reaction yields from nanoparticle clusters," *ACS Photonics*, vol. 7, no. 7, pp. 1885–1892, 2020.
[16] Seiffert L. "Semi-classical description of near-field driven attosecond photoemission from nanostructures," PhD Thesis, Rostock University, 2018.
[17] S. Zherebtsov, F. Süßmann, C. Peltz, et al., "Carrier-envelope phase-tagged imaging of the controlled electron acceleration from SiO_2 nanospheres in intense few-cycle laser fields," *New J. Phys.*, vol. 14, p. 075010, 2012.
[18] L. Seiffert, Q. Liu, S. Zherebtsov, et al., "Attosecond chronoscopy of electron scattering in dielectric nanoparticles," *Nat. Phys.*, vol. 13, pp. 766–770, 2017.
[19] L. Seiffert, F. Süßmann, S. Zherebtsov, et al., "Competition of single and double rescattering in the strong-field photoemission from dielectric nanospheres," *Appl. Phys. B Laser Opt.*, vol. 122, p. 101, 2016.
[20] L. Seiffert, P. Henning, P. Rupp, et al., "Trapping field assisted backscattering in strong-field photoemission from dielectric nanospheres," *J. Mod. Opt.*, vol. 64, pp. 1096–1103, 2017.
[21] N. Kling, D. Paul, A. Gura, et al., "Thick-lens velocity-map imaging spectrometer with high resolution for high-energy charged particles," *J. Instrum.*, vol. 9, no. 05, p. P05005, 2014.
[22] P. Liu, P. J. Ziemann, D. B. Kittelson, and P. H. Mcmurry, "Generating particle beams of controlled dimensions and divergence, ii experimental evaluation of particle motion in aerodynamic lenses and nozzle expansions," *Aerosol. Sci. Technol.*, vol. 22, pp. 314–324, 1995.
[23] Y. Liu, J. Goebl, and Y. Yin, "Templated synthesis of nanostructured materials," *Chem. Soc. Rev.*, vol. 42, no. 7, pp. 2610–2653, 2013.
[24] K. Henrichs, M. Waitz, F. Trinter, et al., "Observation of electron energy discretization in strong field double ionization," *Phys. Rev. Lett.*, vol. 111, p. 113003, 2013.
[25] Y. Shao, M. Li, M. M. Liu, et al., "Isolating resonant excitation from above-threshold ionization," *Phys. Rev. A*, vol. 92, p. 013415, 2015.
[26] F. Süßmann, L. Seiffert, S. Zherebtsov, et al., "Field propagation-induced directionality of carrier-envelope phase-controlled photoemission from nanospheres," *Nat. Commun.*, vol. 6, no. 1, p. 7944, 2015.
[27] P. Rupp, L. Seiffert, Q. Liu, et al., "Quenching of material dependence in few-cycle driven electron acceleration from nanoparticles under many-particle charge interaction," *J. Mod. Opt.*, vol. 64, pp. 995–1003, 2016.
[28] G. Mie, "Beiträge zur optik trüber medien, speziell kolloidaler Metallösungen," *Ann. Phys.*, vol. 25, p. 377, 1908.
[29] D. D. Hickstein, F. Dollar, J. A. Gaffney, et al., "Mapping nanoscale absorption of femtosecond laser pulses using plasma explosion imaging," *ACS Nano*, vol. 8, pp. 8810–8818, 2014.
[30] S. Kim, J. Jin, Y. J. Kim, et al., "High-harmonic generation by resonant plasmon field enhancement," *Nature (London)*, vol. 453, p. 757, 2008.
[31] M. Durach, A. Rusina, M. F. Kling, et al., "Ultrafast dynamic metallization of dielectric nanofilms by strong single-cycle optical fields," *Phys. Rev. Lett.*, vol. 107, p. 086602, 2011.
[32] Q. Liu, L. Seiffert, F. Süßmann, et al., "Ionization-induced subcycle metallization of nanoparticles in few-cycle pulses," *ACS Photonics*, vol. 7, no. 11, pp. 3207–3215, 2020.
[33] U. Saalmann and J. M. Rost, "Ionization of clusters in intense laser pulses through collective electron dynamics," *Phys. Rev. Lett.*, vol. 91, p. 223401, 2003.
[34] T. Döppner, T. Fennel, T. Diederich, et al., "Controlling the Coulomb explosion of silver clusters by femtosecond dual-pulse laser excitation," *Phys. Rev. Lett.*, vol. 94, p. 013401, 2005.
[35] A. E. Kaplan, B. Y. Dubetsky, and P. L. Shkolnikov, "Shock shells in Coulomb explosions of nanoclusters," *Phys. Rev. Lett.*, vol. 91, p. 143401, 2003.